nature geoscience

LETTERS

PUBLISHED ONLINE: 14 APRIL 2013 | DOI: 10.1038/NGEO1792

Patterns of the seasonal response of tropical rainfall to global warming

Ping Huang[1]*, Shang-Ping Xie[2,3,4]*, Kaiming Hu[1], Gang Huang[5] and Ronghui Huang[1]

Tropical convection is an important factor in regional climate variability and change around the globe[1,2]. The response of regional precipitation to global warming is spatially variable, and state-of-the-art model projections suffer large uncertainties in the geographic distribution of precipitation changes[3–5]. Two views exist regarding tropical rainfall change: one predicts increased rainfall in presently rainy regions (wet-get-wetter)[6–8], and the other suggests increased rainfall where the rise in sea surface temperature exceeds the mean surface warming in the tropics (warmer-get-wetter)[9–12]. Here we analyse simulations with 18 models from the Coupled Model Intercomparison Project (CMIP5), and present a unifying view for seasonal rainfall change. We find that the pattern of ocean warming induces ascending atmospheric flow at the Equator and subsidence on the flanks, anchoring a band of annual mean rainfall increase near the Equator that reflects the warmer-get-wetter view. However, this climatological ascending motion marches back and forth across the Equator with the Sun, pumping moisture upwards from the boundary layer and causing seasonal rainfall anomalies to follow a wet-get-wetter pattern. The seasonal mean rainfall, which is the sum of the annual mean and seasonal anomalies, thus combines the wet-get-wetter and warmer-get-wetter trends. Given that precipitation climatology is well observed whereas the pattern of ocean surface warming is poorly constrained[13,14], our results suggest that projections of tropical seasonal mean rainfall are more reliable than the annual mean.

The increase in atmospheric water vapour is a robust change under global warming as relative humidity remains relatively unchanged. The resultant intensification of the vertical moisture gradient, advected by the mean vertical motion, causes rainfall to increase where net water flux at the surface (P–E) is positive, and vice versa (wet-get-wetter)[7]. The enhanced lateral advection calls for reduced precipitation on the margins of a climatological rain band (upped-ante)[6,8]. The wet-get-wetter and upped-ante mechanisms do not emphasize the spatial variations in sea surface temperature (SST) warming. In Coupled Model Intercomparison Project (CMIP) models, the spatial distribution of tropical rainfall response is highly correlated with the overlooked SST pattern[5]. As tropospheric temperature is flattened by fast equatorial waves and set by the tropical mean SST (refs 10,15), local change in convective instability and hence rainfall is determined by relative SST defined as the deviation from the tropical mean (warmer-get-wetter, WaGW)[9,15]. We show that both the WaGW and wet-get-wetter (WeGW) mechanisms are important for tropical rainfall change, dominating the annual mean and seasonal anomalies, respectively. The result has implications for constraining rainfall projection.

The historical simulation and the representative concentration pathway 4.5 (RCP 4.5) experiment from 18 CMIP5 models (see Methods) are used to represent the present and future climates, respectively[16]. Figure 1 shows multi-model ensemble (MME) and zonal mean change in precipitation (P) and SST. The WeGW effect is obvious as ΔP moves back and forth across the Equator following the seasonal cycle of $\bar{P}$ (refs 17,18). (The overbar and Δ denote the present climatology and change in future climate, respectively.) The ocean warming (ΔSST) peaks on the Equator and shows a weak seasonal cycle[9,19]. (Seasonal variations of ΔSST are only 6% of the annual-mean, spatial variations.) On close inspection, the deviations from the WeGW pattern are apparent: precipitation increase (ΔP) exhibits smaller meridional excursions than $\bar{P}$, with the maximum displaced on the equatorward flank of the climatological rain band. The peak rainfall is larger in March than September for ΔP but the opposite is true for $\bar{P}$. We will show that these deviations from WeGW are ΔSST effects. (The upped-ante mechanism calls for rainfall reduction on both margins of the mean convergence zone, and does not explain the consistent equatorward displacement of ΔP relative to $\bar{P}$.)

To isolate the ΔSST effect, we also analyse a pair of additional atmospheric experiments in CMIP5, forced respectively by a spatially uniform SST increase (SUSI) of 4 K and by the spatially patterned SST increase (SPSI) derived from MME CMIP3 quadruple CO_2 (1%to4×) simulations[16,20,21]. The observed SST climatology is used for both runs. The SST warming pattern used in the SPSI run is very similar to ΔSST in RCP 4.5, both with an equatorial peak and a weak seasonal cycle (Supplementary Fig. S1). The SPSI results are scaled by its tropical mean SST increase, so the SPSI minus SUSI difference represents the SST pattern effect under the assumption that the nonlinear dependency on ΔSST amplitude is small.

A band of increased precipitation in SUSI marches across the Equator following $\bar{P}$, and the peak of ΔP coincides with that of $\bar{P}$ (Fig. 2a). This validates the WeGW mechanism. Precipitation change in SPSI is similar to that in RCP 4.5 runs (Figs 2b and 1a) but deviates markedly from SUSI runs. Compared with SUSI, the anomalous rain band in SPSI features small meridional swings and rainfall increase is enhanced near the Equator. The SPSI minus SUSI difference shows only a weak seasonal cycle and is tightly trapped on the Equator, consistent with the ΔSST structure. The ΔSST effect is stronger in the first than in the second half of

[1]Center for Monsoon System Research, Institute of Atmospheric Physics, Chinese Academy of Sciences, Beijing 100190, China, [2]Scripps Institution of Oceanography, University of California at San Diego, La Jolla, California 92093, USA, [3]Physical Oceanography Laboratory, Ocean University of China, Qingdao 266003, China, [4]International Pacific Research Center, University of Hawaii at Manoa, Honolulu, Hawaii 96822, USA, [5]Key Laboratory of Regional Climate-Environment Research for Temperate East Asia, Institute of Atmospheric Physics, Chinese Academy of Sciences, Beijing 100190, China.
*e-mail: huangping@mail.iap.ac.cn; sxie@ucsd.edu.

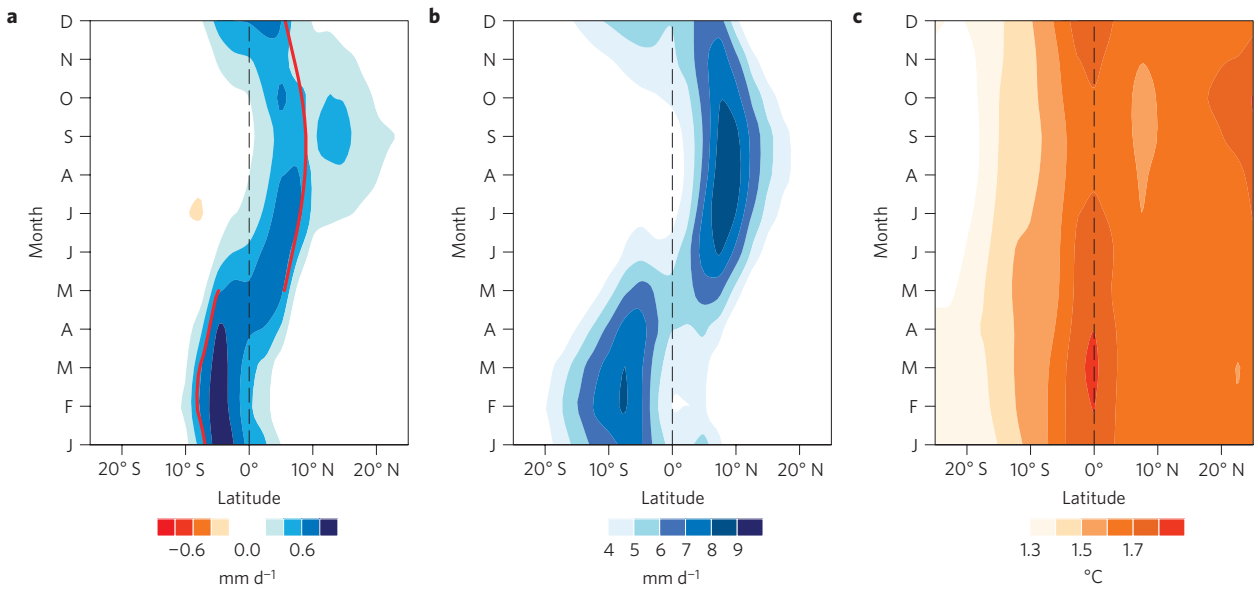

Figure 1 | Seasonal cycle of precipitation and SST change. a–c, Precipitation change (**a**), the precipitation climatology (**b**) and SST change (**c**) in RCP 4.5, all in zonal and MME mean. In **a**, the red curve marks the latitude of the maximum in mean precipitation.

the year because the seasonal development of equatorial upwelling suppresses the SST warming[9].

Vertical velocity change ($\Delta\omega$), overlooked in the WeGW hypothesis, proves important for rainfall change. In SUSI, $\Delta\omega$ broadly represents a weakening of tropical circulation (Fig. 2d) as required by a muted response of global precipitation[8,14]. In SPSI, $\Delta\omega$ is greatly enhanced near the Equator owing largely to the SST effect (Fig. 2e). The SST-induced change in $\Delta\omega$ closely resembles that in ΔP (Fig. 2f,c). The ΔSST peak anchors the anomalous rising motion near the Equator and compensating subsidence on the flanks. Even the weak seasonal cycle is mutually consistent among ΔSST, $\Delta\omega$ and ΔP, modulated to some degree by convective feedback[22]. The time–latitude evolution of $\Delta\omega$ is similar between SPSI and RCP 4.5 runs (Figs 2e and 3a). The ΔSST effect on $\Delta\omega$ can alternatively be understood from a moist instability argument[9]. ΔSST and surface Δq dominate the regional distribution of convective instability change because of the flattened upper tropospheric temperature change[9,10]. Specifically on the Equator where ΔSST peaks, the enhanced convective instability anchors a maximum in precipitation increase and anomalous upward motion.

The water vapour budget can decompose tropical rainfall change into

$$\Delta P \sim \Delta\omega \cdot \bar{q} + \bar{\omega} \cdot \Delta q \qquad (1)$$

where q denotes surface specific humidity, ω is the pressure velocity at 500 hPa, and lateral advection has been neglected, a good approximation for the tropics[7]. Figure 3 shows the decomposition results for RCP 4.5 runs. Equation (1) reproduces ΔP well from full models (Figs 1a and 3d). (The calculation using the full vertical-integrated budget yields nearly identical results.) As both $\bar{q}$ and Δq have broad structures that peak in the climatological rain band (Supplementary Fig. S2), both terms in equation (1) are dominated by vertical velocity in meridional structure (Fig. 3), although the poleward moisture decrease reduces the effect of vertical motion on precipitation away from the deep tropics. The thermodynamic component $\bar{\omega} \cdot \Delta q$ represents the WeGW effect, with the upward motion in the climatological rain band pumping up the moisture increase near the surface. The dynamic component $\Delta\omega \cdot \bar{q}$ causes rainfall to increase (decrease) near (off) the Equator, consistent with the vertical circulation change induced by the equatorial peak in SST warming. We have repeated the decomposition for SUSI and SPSI runs (Supplementary Fig. S3). The results confirm that the dynamic component is due to the SST effect following the WaGW pattern. Remarkably, the thermodynamic component is nearly identical between SUSI and SPSI runs, illustrating that the seasonal cycle in precipitation change is dominated by the WeGW mechanism.

Monthly mean ΔP is significantly correlated with both $\bar{P}$ and ΔSST at 0.67 and 0.60, respectively (Fig. 4), indicating that the WeGW and WaGW mechanisms are both important. The correlation is taken for the seasonal cycle within 10° S–10° N, a latitudinal band that pronounced precipitation change is confined to (Fig. 1a). To illustrate the combined WeGW–WaGW effect, we construct a multi-variant regression

$$\Delta P = a\bar{P} + b(\Delta\mathrm{SST} - c) \qquad (2)$$

for latitude–seasonal variations of zonal and MME means within 10° S and 10° N for 12 months. With $a = 0.11$, $b = 2.23$ and $c = 1.76$, the regression correlates with ΔP from CMIP5 models at 0.89, significantly higher than the correlation with either $\bar{P}$ or ΔSST for the MME analysis. A similar multi-variant regression analysis is performed for each model. The coefficient $a \approx \beta \cdot \langle\Delta\mathrm{SST}\rangle$, where the angle brackets denote the tropical mean and $\beta = 0.07\,\mathrm{K}^{-1}$ is the Clausius–Clapeyron coefficient, represents the thermodynamic effect on ΔP, whereas the coefficient $c \approx \langle\Delta\mathrm{SST}\rangle$ relates the change in the SST threshold for atmospheric convection to the tropical mean SST warming[10] (Supplementary Fig. S4). We use a non-dimensional ratio $\alpha = (b \cdot \sigma(\Delta\mathrm{SST} - c)/a \cdot \sigma(\bar{P}))$ to measure the relative importance of the WaGW to WeGW effect, where σ denotes the standard deviation. For MME, $\alpha = 0.9$, indicating that the WeGW and WaGW effects contribute nearly equally to ΔP. MME average generally underestimates the SST pattern and its effect on rainfall. Indeed the same regression analysis for individual models yields $\alpha > 0.9$ for 13 out of 18 models (Fig. 4d). (Results are not shown for FGOALS-s2 and MIROC5, in which the ΔSST pattern effect is so strong that ΔP is negatively correlated with $\bar{P}$.) The ratio α is significantly correlated with the standard deviation of SST pattern at 0.55 among models, indicating that the stronger the SST pattern is, the greater its relative importance for precipitation change.

In summary, we show that the seasonal precipitation response to global warming is a hybrid of WeGW and WaGW effects (WeWa).

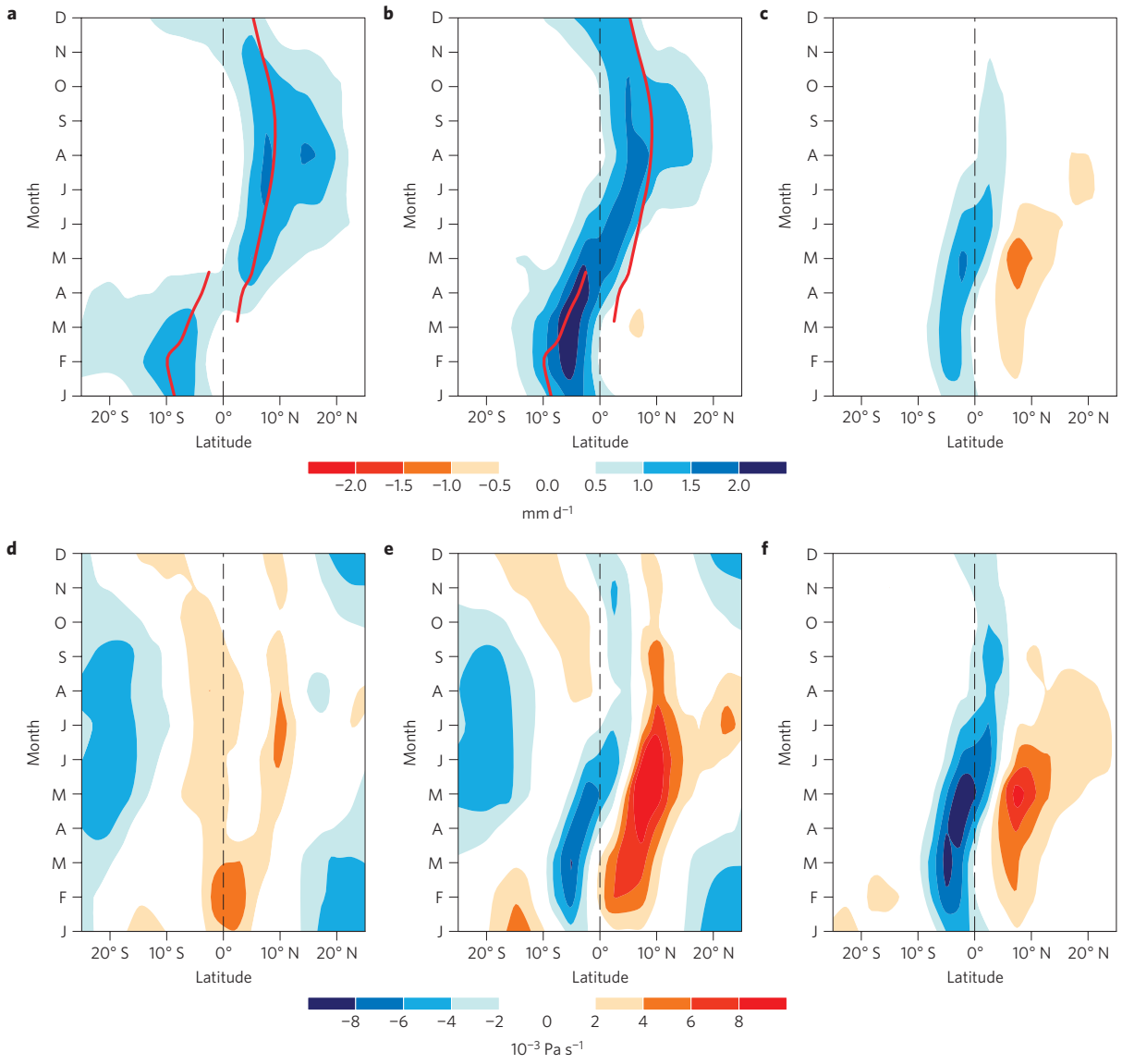

Figure 2 | Seasonal cycle of precipitation and circulation changes in SUSI and SPSI runs. a–c, ΔP in SUSI (**a**) and SPSI (**b**) runs, and their difference (**c**). **d–f**, The same as in **a–c** but for pressure velocity $\Delta\omega$ at 500 hPa. The solid red lines in **a**,**b** mark the latitude of the climatological precipitation maximum in the control. The SPSI results are scaled by the 20° S–20° N mean ΔSST to match SUSI.

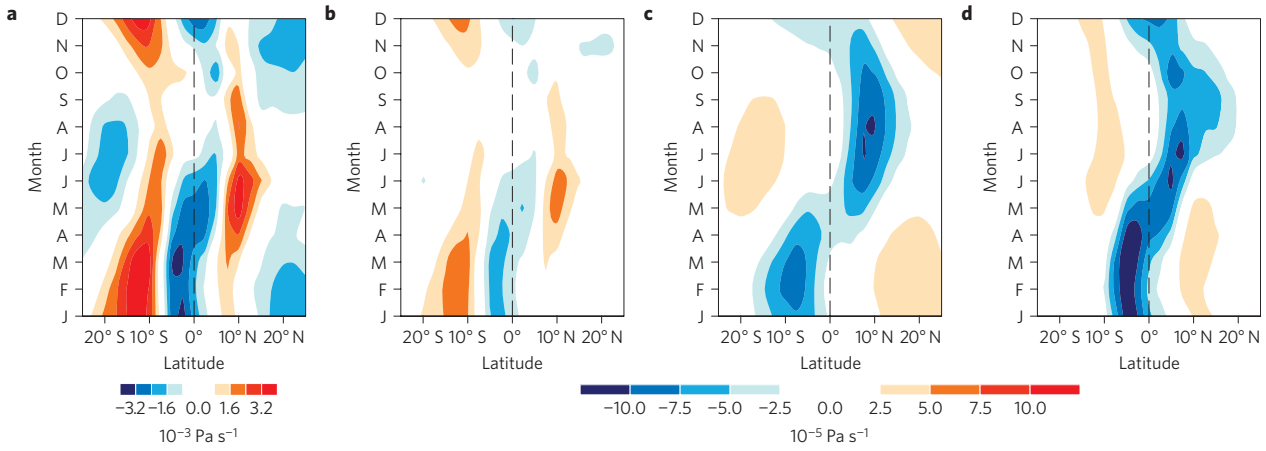

Figure 3 | Circulation change and decomposition of precipitation change. a–d, $\Delta\omega$ at 500 hPa (**a**); dynamic ($\Delta\omega \cdot \bar{q}$) (**b**) and thermodynamic ($\bar{\omega} \cdot \Delta q$) (**c**) components of rainfall change and their sum (**d**).

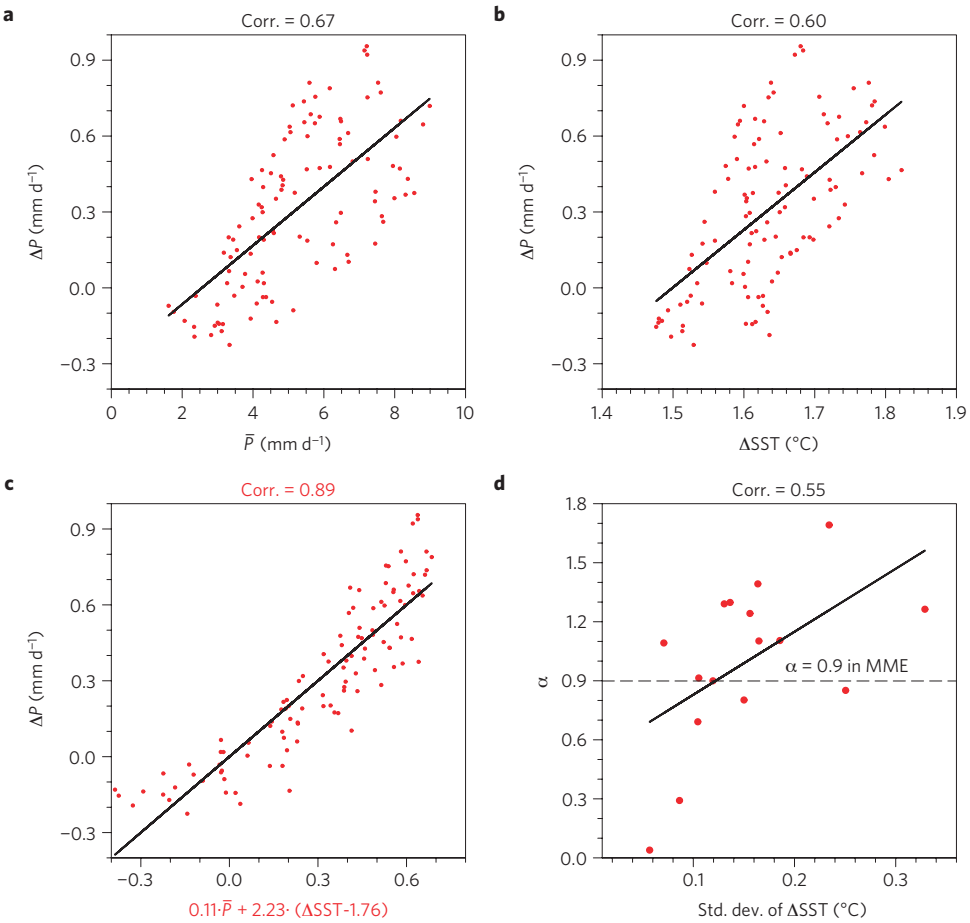

Figure 4 | Relationship of precipitation change to mean precipitation, SST change pattern and their linear combination. a–c, Scatter plots of MME precipitation change with mean precipitation (**a**), SST change (**b**) and their linear combination (equation (2); **c**) in 10° S–10° N through the seasonal cycle. The solid line indicates the linear fit, with the correlation coefficient shown at the top. **d**, The multi-variant regression analysis is also performed for each model, and the ratio α is shown in relation to the spatial standard deviation of ΔSST.

The two effects are not mutually exclusive but complementary, and the combined WeWa view best explains the seasonal precipitation change in the tropics (Fig. 4c). The anomalous rain band moves back and forth across the Equator but is consistently displaced on the equatorward flank of the climatological rain band. The displacement is due to the SST pattern effect. Specifically, the peak of SST warming anchors a band of anomalous ascent and rainfall increase near the Equator. Superimposed on this annual mean pattern, the upward motion in the climatological convergence zone sucks up the moisture increase from the boundary layer like a vacuum cleaner, dragging the band of rainfall increase back and forth across the Equator. We have repeated the linear regression analysis for the annual mean, and two seasons when the climatological rain band is farthest away from the Equator (February–April and August–October). The ratio of the WaGW to WeGW effect α is 1.35, 0.71 and 0.63, respectively (Supplementary Fig. S5). Thus, the WaGW effect is more obvious in the annual mean rainfall change whereas the WeGW effect is more dominant for the seasonal mean.

Regional precipitation projection is important for adaptation but subject to inherent uncertainty much greater than temperature[23,24]. The WeGW and WaGW effects are distinct in the nature of uncertainty regarding regional projection. If the WeGW mechanism dominates, the well-observed climatology can be used to constrain rainfall projection[25]. If the WaGW mechanism were to dominate, on the other hand, the uncertainty would be much greater because the SST warming pattern varies among models[5,26] and is poorly constrained by observations[13,14,27]. In light of the fact that the WeGW effect contributes more to the seasonal than the annual mean rainfall, we suggest that model projection is more reliable for the seasonal than annual mean rainfall in the tropics. This explains why the global monsoon rainfall increases consistently across models[28,29], a change that our results suggest probably takes place, with great environmental and socio-economic impacts.

Methods

CMIP5 models. We use the historical and RCP 4.5 experiments from 18 coupled general circulation models contributing to CMIP5 at http://pcmdi9.llnl.gov/ (ref. 16). They are BCC-CSM1.1, CanESM2, CCSM4, CNRM-CM5, CSIRO-Mk3.6.0, FGOALS-s2, GFDL-CM3, GFDL-ESM2G, GISS-E2-R, HadGEM2-ES, INM-CM4, IPSL-CM5A-LR, IPSL-CM5A-MR, MIROC5, MIROC-ESM, MIROC-ESM-CHEM, MRI-CGCM3 and NorESM1. See http://cmip-pcmdi.llnl.gov/cmip5/availability.html for details. The 1981–2000 mean defines the present climatology, the 2081–2100 mean in RCP 4.5 runs the future climatology, and their difference represents the change under global warming. The MME is defined as the simple average of 18 models.

Output from six atmospheric models (CanAM4, CNRM-CM5, HadGEM2-A, IPSL-CM5A-LR, MIROC5 and MRI-CGCM3) is available for a set of control, SUSI, and SPSI runs, called amip, amip4K and amipFuture in CMIP5, respectively[16,21]. In SUSI, a spatially uniform SST increase of 4 K (constant in time) is superimposed on the observed SST whereas SPSI uses the spatially patterned SST increase derived from the MME CMIP3 quadruple CO_2 (1%to4×) simulation. The SST pattern in SPSI is similar to that in CMIP5 RCP 4.5 runs, both with a peak on the Equator and a weak seasonal cycle (Supplementary Fig. S1 and Fig. 1c). The climate change

is defined as the 20-year monthly climatology for 1981–2000 in SUSI and SPSI runs minus that in the control runs. We scaled the SPSI results so that the tropical mean SST increase is the same as SUSI.

Received 30 October 2012; accepted 6 March 2013; published online 14 April 2013

References

1. Alexander, M. A. *et al.* The atmospheric bridge: The influence of ENSO teleconnections on air–sea interaction over the global oceans. *J. Clim.* **15,** 2205–2231 (2002).
2. Shin, S-I. & Sardeshmukh, P. D. Critical influence of the pattern of Tropical Ocean warming on remote climate trends. *Clim. Dyn.* **36,** 1577–1591 (2011).
3. Meehl, G. A. *et al.* in *Climate Change 2007: The Physical Science Basis* (eds Solomon, S. *et al.*) Ch. 10, 747–845 (Global Climate Projections, Cambridge Univ. Press, 2007).
4. Zhang, X. *et al.* Detection of human influence on twentieth-century precipitation trends. *Nature* **448,** 461–465 (2007).
5. Ma, J. & Xie, S-P. Regional patterns of sea surface temperature change: A source of uncertainty in future projections of precipitation and atmospheric circulation. *J. Clim.* http://dx.doi.org/10.1175/JCLI-D-1112-00283.00281 (in the press, 2013).
6. Neelin, J., Chou, C. & Su, H. Tropical drought regions in global warming and El Nino teleconnections. *Geophys. Res. Lett.* **30,** 2275 (2003).
7. Held, I. M. & Soden, B. J. Robust responses of the hydrological cycle to global warming. *J. Clim.* **19,** 5686–5699 (2006).
8. Chou, C., Neelin, J., Chen, C. & Tu, J. Evaluating the 'rich-get-richer' mechanism in tropical precipitation change under global warming. *J. Clim.* **22,** 1982–2005 (2009).
9. Xie, S-P. *et al.* Global warming pattern formation: Sea surface temperature and rainfall. *J. Clim.* **23,** 966–986 (2010).
10. Johnson, N. C. & Xie, S-P. Changes in the sea surface temperature threshold for tropical convection. *Nature Geosci.* **3,** 842–845 (2010).
11. Sobel, A. H. & Camargo, S. J. Projected future seasonal changes in tropical summer climate. *J. Clim.* **24,** 473–487 (2011).
12. Chadwick, R., Boutle, I. & Martin, G. Spatial patterns of precipitation change in CMIP5: Why the rich don't get richer in the tropics. *J. Clim.* http://dx.doi.org/10.1175/JCLI-D-1112-00543.00541 (in the press, 2013).
13. Tokinaga, H., Xie, S. P., Deser, C., Kosaka, Y. & Okumura, Y. M. Slowdown of the Walker circulation driven by tropical Indo-Pacific warming. *Nature* **491,** 439–443 (2012).
14. Vecchi, G. & Soden, B. Global warming and the weakening of the tropical circulation. *J. Clim.* **20,** 4316–4340 (2007).
15. Vecchi, G. A. & Soden, B. J. Effect of remote sea surface temperature change on tropical cyclone potential intensity. *Nature* **450,** 1066–1070 (2007).
16. Taylor, K. E., Stouffer, R. J. & Meehl, G. A. An overview of CMIP5 and the experiment design. *Bull. Am. Meteorol. Soc.* **93,** 485–498 (2012).
17. Chou, C. & Tu, J. Y. Hemispherical asymmetry of tropical precipitation in ECHAM5/MPI-OM during El Niño and under global warming. *J. Clim.* **21,** 1309–1332 (2008).
18. Tan, P-H., Chou, C. & Tu, J-Y. Mechanisms of global warming impacts on robustness of tropical precipitation asymmetry. *J. Clim.* **21,** 5585–5602 (2008).
19. Liu, Z., Vavrus, S., He, F., Wen, N. & Zhong, Y. Rethinking tropical ocean response to global warming: The enhanced equatorial warming. *J. Clim.* **18,** 4684–4700 (2005).
20. Cess, R. D. *et al.* Intercomparison and interpretation of climate feedback processes in 19 atmospheric general circulation models. *J. Geophys. Res.* **95,** 601216 (1990).
21. Bony, S. *et al.* CFMIP: Towards a better evaluation and understanding of clouds and cloud feedbacks in CMIP5 models. *CLIVAR Exchanges* **56,** 20–24 (2011).
22. Watanabe, M. & Jin, F. F. A moist linear baroclinic model: Coupled dynamical-convective response to El Nino. *J. Clim.* **16,** 1121–1139 (2003).
23. Lau, K. M. & Wu, H. T. Detecting trends in tropical rainfall characteristics, 1979–2003. *Int. J. Climatol.* **27,** 979–988 (2007).
24. Wentz, F. J., Ricciardulli, L., Hilburn, K. & Mears, C. How much more rain will global warming bring? *Science* **317,** 233–235 (2007).
25. Allan, R. P., Soden, B. J., John, V. O., Ingram, W. & Good, P. Current changes in tropical precipitation. *Environ. Res. Lett.* **5,** 025205 (2010).
26. Lu, J. & Zhao, B. The role of oceanic feedback in the climate response to doubling CO_2. *J. Clim.* **25,** 7544–7563 (2012).
27. Deser, C., Phillips, A. & Alexander, M. Twentieth century tropical sea surface temperature trends revisited. *Geophys. Res. Lett.* **37,** L10701 (2010).
28. Hsu, P. C. *et al.* Increase of global monsoon area and precipitation under global warming: A robust signal? *Geophys. Res. Lett.* **39,** L06701 (2012).
29. Kitoh, A. *et al.* Monsoons in a changing world: a regional perspective in a global context. *J. Geophys. Res.* http://dx.doi.org/10.1002/jgrd.50258 (2013).

Acknowledgements

The work was supported by the National Basic Research Program of China (2012CB955604 and 2010CB950403), the Natural Science Foundation of China (41105047 and 41275083) and the US National Science Foundation. We wish to thank C. Chou for helpful discussions, and X. Qu for data processing. We acknowledge the World Climate Research Programme's Working Group on Coupled Modelling, which is responsible for CMIP5, and we thank the climate modeling groups (listed in the Methods of this paper) for producing and making available their model output.

Author contributions

P.H. designed and performed the analysis. S-P.X. contributed to improving the analysis and interpretation. K.H. and G.H. prepared part of the data. P.H. and S-P.X. wrote the paper. All authors discussed and commented on the paper.

Additional information

Supplementary information is available in the online version of the paper. Reprints and permissions information is available online at www.nature.com/reprints. Correspondence and requests for materials should be addressed to P.H. or S-P.X.

Competing financial interests

The authors declare no competing financial interests.